

# The elastoplastic response of and moisture diffusion through a vinyl ester resin–clay nanocomposite

A.D. Drozdov, J. deC. Christiansen

Department of Production

Aalborg University

Fibigerstraede 16

DK-9220 Aalborg, Denmark

and

R.K. Gupta, A.P. Shah\*

Department of Chemical Engineering and Constructed Facilities Center

West Virginia University

P.O. Box 6102

Morgantown, WV 26506, USA

## Abstract

Experimental data are reported on the elastoplastic response of and moisture diffusion through a vinyl ester resin–montmorillonite clay nanocomposite with various amounts of filler. Two simple models are developed for the elastoplastic behavior of a nanocomposite and for the anomalous diffusion of penetrant molecules. Adjustable parameters in the constitutive equations are found by fitting the observations. It is revealed that some critical concentration of filler exists (about 1 wt.-%): in the sub-critical region of concentrations, molecular mobility of the host polymer strongly decreases with the clay content, whereas in the post-critical domain, the filler fraction weakly affects mobility of chains.

**Key-words:** Nanocomposite, Elastoplasticity, Anomalous diffusion

---

\*Present address: Triton Systems Inc., 200 Turnpike Road, Chelmsford, MA 01824, USA

# 1 Introduction

This paper is concerned with the elastoplastic behavior of and moisture diffusion through a nanocomposite consisting of a vinyl ester resin matrix filled with montmorillonite clay particles.

The choice of vinyl ester resin is explained by the fact that this thermosetting polymer is widely used as a matrix for glass-reinforced polymer composites employed for construction and repair of bridges and other civil structures (Valea et al., 1998; Patel et al., 1999).

Montmorillonite (MMT) is a commonly used clay with a layered structure that is constructed of two tetrahedral sheets of silica surrounding an octahedral sheet of alumina or magnesia (Masenelli-Varlot et al., 2002). The layers (with thickness of 1 nm) are stacked by weak dipole forces, while the galleries between the layers are occupied by metal cations. Processing of clay particles for preparation of an intercalated nanocomposite consists of two stages:

1. The growth of the basal (interlayer) spacing by exchanging the metal cations with an intercalating reagent (conventionally, alkylammonium ions). This process facilitates intercalation of polymer chains into the galleries between the clay layers (Chang et al., 2002).
2. Treatment of intercalated particles by a compatibilizer (a swelling agent, a functional oligomer, or a low molecular weight polymer) to improve miscibility between the organics-modified silicate layers and the host matrix (Tyan et al., 2000; Ma et al., 2001; Chang et al., 2002).

Preparation and analysis of micro-structure and physical properties of nanocomposites with polymeric matrices filled with MMT clay have been a focus of attention in the past couple of years. It was found that polymer–clay nanocomposites possess many desirable properties, such as increased moduli and strength, reduced gas permeabilities, decreased adsorption of organic liquids, etc. (Kim et al., 2002). However, no detailed analysis of interaction between molecules of a host matrix and the silica sheets has been performed so far.

The objective of the present study is to investigate how the presence of intercalated MMT clay affects the mobility of polymeric chains. We focus on two main processes, where this mobility is revealed:

1. elastoplasticity (which is attributed to sliding of junctions in the polymeric network with respect to their reference positions in the bulk material),
2. moisture diffusion (whose rate is governed by the ability of penetrant molecules to move through the host network).

In civil engineering applications, these two processes are of essential importance for the prediction of durability and performance of constructions.

To evaluate the effect of nano-particles on the mobility of macromolecules, we focus on a model nanocomposite where no compatibilizer is used. Because of low miscibility

between the clay particles and the vinyl ester resin, we do not expect that the presence of intercalated clay particles noticeably improves the mechanical and transport properties of a nanocomposite compared to those of the neat resin (Ma et al., 2001). Our aim is to demonstrate that the concentration of nano-particles affects the parameters that characterize mobility of polymeric chains in mechanical and diffusion tests in similar ways.

In the past two decades, a number of constitutive models have been proposed for the elastoplastic and viscoplastic behavior of glassy polymers, see, e.g., Boyce et al. (1988), Mangion et al. (1992), Hasan and Boyce (1995), David et al. (1997), Drozdov (2001) and the references therein. Three shortcomings of these models should be mentioned:

- the stress-strain relations were developed to correctly describe the mechanical behavior of polymers near the yield point (which is not the case for vinyl ester resin where fracture occurs earlier than yielding, see Figures 1 to 5 below),
- the constitutive equations contain a number of adjustable parameters which cannot be determined with a high level of accuracy by fitting data in uniaxial tensile tests,
- the material constants are not explicitly expressed in terms of the physical quantities that describe molecular mobility.

To assess constraints imposed by the clay particles on the mobility of macromolecules in a host matrix, we develop a simple model that contains only three adjustable parameters with a transparent physical meaning. Only one of these parameters reflects mobility of chains, and it can be easily found by fitting stress-strain curves in uniaxial tensile tests with small strains.

Diffusion of moisture in polymer composites has attracted substantial attention in the past decade, see, e.g., Cai and Weitsman (1994), Bavisi et al. (1996), Vanlandingham et al. (1999), Marcovich et al. (1999), Roy et al. (2000), Chen et al. (2001), Roy et al. (2001), Uschitsky and Suhir (2001), to mention a few. It was demonstrated that diffusion of penetrants in several glassy polymers is anomalous (non-Fickian), with the mass gain proportional to some power of time that differs from 0.5 (the latter is characteristic for the Fickian diffusion).

Two approaches were recently proposed to model the anomalous diffusion. According to the first (the fractional dynamics concept), conventional derivatives with respect to time and spatial variables in the diffusion equation are replaced by fractional derivatives, see Metzler and Klafter (2000) and the references therein. According to the other (Roy et al., 2000), a constant coefficient of diffusion is replaced by a decreasing function of time (by analogy with a relaxation modulus for a viscoelastic solid).

Our experimental data (see Figures 6 to 10 below) reveal that moisture diffusion in the neat vinyl ester resin is practically Fickian, while the anomalous transport of water molecules is observed with an increase in the clay concentration. This phenomenon may be explained by the fact that the water molecules are bounded to hydrophilic surfaces of clay layers, where they become immobilized. A two-stage diffusion process with immobilization of penetrant molecules has been previously studied by Carter and Kibler (1978) and Gurtin and Yatomi (1979). Unlike these works, we assume that bounded molecules

cannot leave the sites where they were immobilized. This allows the number of adjustable parameters to be substantially reduced. The diffusion process is governed by differential equations with only three material constants that are found by matching the water uptake curves plotted in Figures 6 to 10.

The exposition is organized as follows. Observations in uniaxial tensile tests and in moisture diffusion tests are reported in Section 2. Constitutive equations for the elasto-plastic response are derived in Section 3 by using the laws of thermodynamics. Adjustable parameters in these relations are determined in Section 4. A model for moisture diffusion is developed in Section 5 and its material constants are found in Section 6. A brief discussion of our findings is presented in Section 7. Some concluding remarks are formulated in Section 8.

## 2 Experimental procedure

### 2.1 Preparation of samples

The polymer used was DERAKANE 411-350 epoxy vinyl ester resin (Dow Chemical Co.) containing 45 wt.-% of dissolved styrene. To cure the resin at room temperature, it was mixed with 0.5 wt.-% of 6% cobalt naphthenate catalyst (Sigma Aldrich Co.). Additionally, 0.05% of 99% N,N dimethyl aniline (Lancaster Synthesis, Pelham, NH, USA) was used as an accelerator, and 1.5% of methyl ethyl ketone peroxide with 9% of active oxygen (Sigma Aldrich Co.) as an initiator.

A montmorillonite clay Cloisite 10A (Southern Clay Products Inc., Gonzales, TX, USA) treated with benzyl (hydrogenated tallow alkyl) dimethyl quaternary ammonium chloride was used as received. Neat resin coupons were cast by pouring the reaction mixture into Teflon molds with the dimensions  $50 \times 12.5$  mm and the thickness ranging from 0.2 to 0.6 mm. The organically treated clay was added to the liquid resin and manually stirred. The mixture was then degassed in a vacuum oven to remove air bubbles. Afterwards, the catalyst, initiator and accelerator were added. The mixture was allowed to cure at room temperature for 24 hours, and it was subsequently post cured in an oven for 3 hours at 90 °C.

TEM (transmission electron microscopy) micrographs of the nanocomposite samples show that the clay is reasonably uniformly distributed, and the silica sheets are randomly oriented (Shah et al., 2002). The clay exists as expanded aggregates made up of 2 to 10 sheets with the interlayer distance ranging from 4.4 to 5.0 nm, which confirms the formation of an intercalated nanocomposite.

### 2.2 Mechanical tests

Dumbbell specimens for mechanical tests were cut following ASTM D638 specification. Tensile tests were performed at ambient temperature by using a 100 kN Instron machine model 8501 with a cross-head speed of 0.254 mm/min. This strain rate ensures practically isothermal loading conditions. The strain was measured independently using a strain gauge affixed to the mid-point of the specimen. The tensile force was measured by a standard load cell. The engineering stress,  $\sigma$ , was determined as the ratio of the tensile

force to the cross-sectional area of a specimen in the stress-free state. For any concentration of filler in a nanocomposite,  $\nu$ , four specimens were tested. Typical stress-strain diagrams are presented in Figures 1 to 5. These figures demonstrate that the response of the neat resin is strongly nonlinear, but the nonlinearity of the stress-strain curves is reduced with an increase in the filler content.

DSC (differential scanning calorimetry) measurements show that the glass transition temperature of the neat vinyl ester resin is about 97 °C, and it increases with concentration of clay reaching 117 °C at  $\nu = 5.0$  wt.-% (Shah et al., 2002). Because the material at room temperature is far below its glass transition point, we disregard its viscoelastic response and attribute the nonlinearity of the stress-strain curves to the elastoplastic behavior.

### 2.3 Diffusion tests

Diffusion tests were performed by immersing samples with rectangular cross-section in distilled water at room temperature ( $T = 25$  °C). The samples had a dry mass ranging from 120 to 400 mg. They were stored in a controlled humidity chamber, and contained  $0.05 \pm 0.005$  wt.-% water at the beginning of diffusion tests. The samples were periodically removed, blotted dry with a lint-free tissue, weighed and re-immersed in the water. A typical experiment lasted ten days, and, on the first day, readings were taken as frequently as every 15 min. The balance used had an accuracy of 1 mg, and 3 to 5 replicate runs were carried out for a given set of condition. Typical dependences of the relative moisture uptake,  $\Phi$ , versus the reduced time,  $\bar{t}$ , are plotted in Figures 6 to 10. The reduced time,  $\bar{t}$ , is given by

$$\bar{t} = \frac{t}{4l^2}, \quad (1)$$

where  $t$  is time elapsed from the beginning of a test, and  $2l$  is thickness of a sample. The relative moisture uptake,  $\Phi$ , is defined as

$$\Phi(\bar{t}) = \frac{R(\bar{t})}{R(\infty)}, \quad (2)$$

where  $R(\bar{t})$  is the mass gain at the reduced time  $\bar{t}$  and  $R(\infty)$  is the maximal mass gain. Observations on samples with various thicknesses (not presented) show that the mass gain curves plotted in the reduced coordinates  $(\Phi, \bar{t})$  are superposed fairly well.

Figures 6 to 10 demonstrate that moisture diffusion in the neat resin is roughly Fickian, but it becomes strongly anomalous with an increase in the filler content.

The aim of the remaining part of this work is to develop constitutive equations for the elastoplastic behavior and moisture diffusion in a nanocomposite and to find adjustable parameters in these relations by matching the experimental data plotted in Figures 1 to 10.

## 3 A model for the elastoplastic response

To simplify the analysis, we model a nanocomposite as an equivalent network of macromolecules bridged by junctions (entanglements, physical cross-links and particles of filler).

Because the viscoelastic behavior of the nanocomposite is disregarded, the network is treated as permanent (we suppose that active chains do not separate from junctions and dangling chains do not merge with the network within the experimental time-scale). To describe the elastoplastic behavior of the network, we assume that junctions slide with respect to their reference positions in the bulk material. For uniaxial deformation, sliding of junctions is determined by a plastic strain  $\epsilon_p$ . Adopting the conventional hypothesis that the macro-strain,  $\epsilon$ , is transmitted to all chains in the network by surrounding macromolecules, we write

$$\epsilon = \epsilon_e + \epsilon_p, \quad (3)$$

where  $\epsilon_e$  is an elastic strain. We accept the mean-field approach and treat  $\epsilon_e$  and  $\epsilon_p$  as average elastic and plastic strains per chain.

It is assumed that under active loading, the rate of changes in the strain,  $\epsilon_p$ , with time,  $t$ , is proportional to the rate of changes in the macro-strain  $\epsilon$ ,

$$\frac{d\epsilon_p}{dt}(t) = \varphi(\epsilon_e(t)) \frac{d\epsilon}{dt}(t), \quad (4)$$

where the coefficient of proportionality,  $\varphi$ , is a function of the elastic strain  $\epsilon_e$ .

The following restrictions are imposed on the function  $\varphi(\epsilon_e)$ :

1. The coefficient of proportionality in Eq. (4) vanishes at the zero elastic strain,  $\varphi(0) = 0$ .
2. The function  $\varphi$  monotonically increases with  $\epsilon_e$  and tends to some constant  $a \in (0, 1)$  for relatively large elastic strains,

$$\lim_{\epsilon_e \rightarrow \infty} \varphi(\epsilon_e) = a.$$

The constant  $a$  determines the rate of sliding in junctions at the stage of a developed plastic flow.

To approximate experimental data, we use the function

$$\varphi(\epsilon_e) = a \left[ 1 - \exp\left(-\frac{\epsilon_e}{e}\right) \right], \quad (5)$$

which satisfies the above conditions. This function is determined by two adjustable parameters,  $a$  and  $e$ , where  $a$  is the limiting value of  $\varphi$  at “large” elastic strains, and  $e > 0$  is a constant that characterizes how “large” an elastic strain,  $\epsilon_e$ , is.

A chain is modelled as a linear elastic solid with the mechanical energy

$$w = \frac{1}{2} \mu \epsilon_e^2,$$

where  $\mu$  is an average rigidity per chain. Multiplying the energy,  $w$ , by the number of chains per unit volume,  $n_0$ , we find the strain energy density

$$W = \frac{1}{2} E \epsilon_e^2, \quad (6)$$

where  $E = \mu n_0$  is an elastic modulus. It is worth noting that the elastic modulus,  $E$ , may differ from the Young modulus. The latter is conventionally defined as the tangent of the angle between the tangent straightline to the stress-strain curve at small strains and the horizontal axis. These two quantities coincide when the elastic strain,  $\epsilon_e$ , is equal to the macro-strain,  $\epsilon$ . For the elasto-plastic response of a nanocomposite, when the stress-strain diagram substantially differs from a straightline,  $E$  exceeds the Young modulus determined by the traditional method.

For isothermal uniaxial deformation, the Clausius-Duhem inequality reads,

$$Q(t) = -\frac{dW}{dt}(t) + \sigma(t) \frac{d\epsilon}{dt}(t) \geq 0,$$

where  $Q$  is internal dissipation per unit volume. Substitution of Eqs. (3), (4) and (6) into this formula results in

$$Q(t) = \left[ \sigma(t) - E\epsilon_e(t)(1 - \varphi(\epsilon_e(t))) \right] \frac{d\epsilon}{dt}(t) \geq 0.$$

Assuming the expression in square brackets to vanish, we arrive at the stress-strain relation

$$\sigma(t) = E\epsilon_e(t)[1 - \varphi(\epsilon_e(t))]. \quad (7)$$

Constitutive equations (3) to (5) and (7) are determined by 3 adjustable parameters:

1. the elastic modulus  $E$ ,
2. the rate of developed plastic flow  $a$ ,
3. the strain,  $e$ , that characterizes transition to the steady-state plastic deformation.

To find these quantities, we match experimental data depicted in Figures 1 to 5.

## 4 Fitting observations in mechanical tests

It follows from Eqs. (3), (4), (5) and (7) that in a uniaxial tensile test, the stress is given by

$$\sigma(\epsilon) = E(\epsilon - \epsilon_p) \left\{ 1 - a \left[ 1 - \exp \left( -\frac{\epsilon - \epsilon_p}{e} \right) \right] \right\}, \quad (8)$$

where the plastic strain,  $\epsilon_p$ , satisfies the nonlinear differential equation

$$\frac{d\epsilon_p}{d\epsilon}(\epsilon) = a \left[ 1 - \exp \left( -\frac{\epsilon - \epsilon_p}{e} \right) \right] \quad (9)$$

with the initial condition  $\epsilon_p(0) = 0$ .

We begin with matching the experimental data in a test on the neat vinyl ester resin, see Figure 1. To find the material constants,  $E$ ,  $a$  and  $e$ , we fix some intervals  $[0, a_{\max}]$  and  $[0, e_{\max}]$ , where the “best-fit” parameters  $a$  and  $e$  are assumed to be located, and divide these intervals into  $I$  subintervals by the points  $a_i = i\Delta a$  and  $e_j = j\Delta e$  ( $i, j = 1, \dots, I$ ) with  $\Delta a = a_{\max}/I$  and  $\Delta e = e_{\max}/I$ . For any pair,  $\{a_i, e_j\}$ , we integrate Eq. (9)

numerically (with the step  $\Delta\epsilon = 1.0 \cdot 10^{-5}$ ) by the Runge–Kutta method. Given  $\{a_i, e_j\}$ , the elastic modulus  $E = E(i, j)$  is found by the least-squares technique from the condition of minimum of the function

$$F(i, j) = \sum_{\epsilon_k} \left[ \sigma_{\text{exp}}(\epsilon_k) - \sigma_{\text{num}}(\epsilon_k) \right]^2,$$

where the sum is calculated over all experimental points,  $\epsilon_k$ , depicted in Figure 1,  $\sigma_{\text{exp}}$  is the stress measured in a tensile test, and  $\sigma_{\text{num}}$  is given by Eq. (8). The “best-fit” parameters  $a$  and  $e$  minimize the function  $F$  on the set  $\{a_i, e_j \quad (i, j = 1, \dots, I)\}$ . Fitting the observations results in  $e = 2.11 \cdot 10^{-3}$ .

We fix this value of  $e$  and proceed with matching observations in tensile tests on other specimens by using only two material constants,  $E$  and  $a$ , which are determined by the above algorithm. The average values of  $E$  and  $a$  (over 4 samples) are depicted in Figures 11 and 12, where the vertical bars stand for the standard deviations of these parameters.

Afterwards, we match experimental data in tensile tests on specimens with various contents of filler,  $\nu$ . The same algorithm of fitting is employed with the fixed value  $e = 2.11 \cdot 10^{-3}$ . Figures 1 to 5 demonstrate fair agreement between the observations and the results of numerical simulation. The elastic modulus,  $E$ , and the rate of developed plastic flow,  $a$ , are plotted versus the filler content,  $\nu$ , in Figures 11 and 12. The experimental data are approximated by the phenomenological equations

$$E = E_0 - E_1 \nu, \quad a = a_0 - a_1 \nu, \quad (10)$$

where the coefficients  $E_j$  and  $a_j$  ( $j = 0, 1$ ) are found by the least-squares technique.

## 5 A model for the moisture diffusion

A sample is treated as a rectilinear plate with thickness  $2l$ . We introduce Cartesian coordinates  $\{x, y, z\}$ , where the axis  $x$  is perpendicular to the middle plane of the plate, and the axes  $y$  and  $z$  lie in the middle plane. Length and width of the plate are assumed to substantially exceed its thickness, which implies that the moisture concentration depends on the coordinate  $x$  only.

After the plate is immersed into water, three processes occur in the composite material:

1. sorption of water molecules to the plate faces from the surrounding,
2. diffusion of the penetrant into the plate,
3. adsorption of water molecules on the surfaces of clay layers, where these molecules become immobilized.

It is conventionally accepted that the rate of sorption in glassy polymers noticeably exceeds the rate of diffusion (Chen et al., 2001), which implies that the sorption equilibrium is rapidly established. The equilibrium condition is given by

$$n(t, x) \Big|_{x=\pm l} = n^\circ, \quad (11)$$

where  $n$  is the moisture concentration at time  $t$  at point  $x$  [the number of water molecules in the polymeric matrix occupying a volume with the unit area in the plane  $(y, z)$  and the thickness  $dx$  reads  $n(t, x)dx$ ], and  $n^\circ$  is the equilibrium moisture concentration in the matrix on the faces of the plate.

Diffusion of the penetrant through the matrix is described by the mass conservation law

$$\frac{\partial n}{\partial t} = \frac{\partial J}{\partial x} - \frac{\partial n_1}{\partial t}, \quad (12)$$

where  $J(t, x)$  stands for the mass flux, and  $n_1(t, x)$  denotes the concentration of water molecules immobilized at the surfaces of clay layers.

The mass flux obeys the Fick equation

$$J = D \frac{\partial n}{\partial x}, \quad (13)$$

where  $D$  is diffusivity. Equation (13) is tantamount to the assumption that diffusion occurs through the polymeric matrix only. However, the coefficient of diffusion,  $D$ , is assumed to depend on the volume content of filler, because the presence of particles results in a decay in the molecular mobility of polymeric molecules which provides the driving force for diffusion of penetrants.

Adsorption of water molecules on the surfaces of filler is determined by the first-order kinetic equation

$$\frac{\partial n_1}{\partial t} = kn(n_1^\circ - n_1). \quad (14)$$

According to Eq. (14), the rate of adsorption is proportional to the concentration of the penetrant in the matrix,  $n$ , and to the current number of “unoccupied sites” on the surfaces of filler,  $n_1^\circ - n_1$ , where  $n_1^\circ$  is the total number of sites where water molecules can be immobilized. In the general case, the rate of adsorption,  $k$ , and the maximal concentration of unoccupied sites,  $n_1^\circ$ , are functions of the clay content, because the presence of nanoparticles affect mobility of chains in the polymeric matrix, and, as a consequence, their chemical potential.

Neglecting the moisture content in a sample before testing, we adopt the following initial conditions:

$$n(t, x) \Big|_{t=0} = 0, \quad n_1(t, x) \Big|_{t=0} = 0. \quad (15)$$

Equations (12) to (14) with initial conditions (15) and boundary condition (11) uniquely determine the diffusion process. The moisture mass gain (per unit mass of the sample) is given by

$$R(t) = \frac{\kappa}{2l\rho} \int_{-l}^l [n(t, x) + n_1(t, x)] dx, \quad (16)$$

where  $\kappa$  is the average mass of a penetrant molecule, and  $\rho$  is mass density of the matrix.

Our aim now is to transform Eqs. (11) to (16). For this purpose, we introduce the dimensionless coordinate,  $\bar{x} = x/l$ , and the reduced moisture concentrations,  $c = n/n^\circ$  and  $c_1 = n_1/n^\circ$ . Combining Eqs. (1), (12) and (13), we arrive at the mass flux equation

$$\frac{\partial c}{\partial \bar{t}} = \bar{D} \frac{\partial^2 c}{\partial \bar{x}^2} - \frac{\partial c}{\partial \bar{t}}, \quad (17)$$

where

$$\bar{D} = 4D. \quad (18)$$

In the new notation, Eq. (14) reads

$$\frac{\partial c_1}{\partial \bar{t}} = Kc(C - c_1), \quad (19)$$

where

$$K = 4kl^2n^\circ, \quad C = \frac{n_1^\circ}{n^\circ}. \quad (20)$$

Initial conditions (15) remain unchanged,

$$c(0, \bar{x}) = 0, \quad c_1(0, \bar{x}) = 0. \quad (21)$$

Bearing in mind that the functions  $c(\bar{t}, \bar{x})$  and  $c_1(\bar{t}, \bar{x})$  are even functions of  $\bar{x}$ , we present boundary condition (11) in the form

$$\frac{\partial c}{\partial \bar{x}}(\bar{t}, 0) = 0, \quad c(\bar{t}, 1) = 1. \quad (22)$$

Finally, Eq. (16) is given by

$$R(\bar{t}) = \frac{\kappa}{\rho} n^\circ \int_0^1 [c(\bar{t}, \bar{x}) + c_1(\bar{t}, \bar{x})] d\bar{x}. \quad (23)$$

With an increase in time,  $\bar{t}$ , the solutions of Eqs. (17) and (19) tend to the steady-state solutions

$$c(\infty, \bar{x}) = 1, \quad c_1(\infty, \bar{x}) = C. \quad (24)$$

It follows from Eqs. (23) and (24) that the maximal moisture uptake reads

$$R(\infty) = \frac{\kappa}{\rho} n^\circ (1 + C), \quad (25)$$

whereas the relative mass gain, see Eq. (2), is given by

$$\Phi(\bar{t}) = \frac{1}{1 + C} \int_0^1 [c(\bar{t}, \bar{x}) + c_1(\bar{t}, \bar{x})] d\bar{x}. \quad (26)$$

Equations (17), (19) and (26) with initial conditions (21) and boundary conditions (22) are determined by 3 adjustable parameters:

1. the reduced diffusivity  $\bar{D}$ ,
2. the rate of moisture adsorption on nanoparticles  $K$ ,
3. the reduced concentration of unoccupied sites on the surfaces of filler  $C$ .

These constants are found by fitting the experimental data in diffusion tests.

## 6 Fitting observations in diffusion tests

We begin with matching the experimental data for the neat vinyl resin depicted in Figure 6. Because in the absence of filler, moisture is not adsorbed on the surfaces of particles, we set  $C = 0$  in Eq. (17). Equations (17), (21) and (22) are reduced to the conventional boundary problem for the diffusion equation

$$\frac{\partial c}{\partial \bar{t}} = \bar{D} \frac{\partial^2 c}{\partial \bar{x}^2}, \quad \frac{\partial c}{\partial \bar{x}}(\bar{t}, 0) = 0, \quad c(\bar{t}, 1) = 1, \quad c(0, \bar{x}) = 0, \quad (27)$$

which is resolved by the finite-difference method with an explicit algorithm. Given a coefficient of diffusion,  $\bar{D}$ , we divide the interval  $[0, 1]$  into  $M$  subintervals by points  $\bar{x}_m = m\Delta x$  ( $m = 0, 1, \dots, M$ ) with  $\Delta x = 1/M$ , introduce discrete time  $\bar{t}_n = n\Delta t$ , and replace Eq. (27) by its finite-difference approximation

$$\begin{aligned} c(0, \bar{x}_m) &= 0 \quad (m = 0, 1, \dots, M-1), & c(0, \bar{x}_M) &= 1, \\ c(\bar{t}_{n+1}, \bar{x}_m) &= c(\bar{t}_n, \bar{x}_m) + \bar{D} \frac{\Delta t}{\Delta x^2} \left[ c(\bar{t}_n, \bar{x}_{m+1}) - 2c(\bar{t}_n, \bar{x}_m) \right. \\ &\quad \left. + c(\bar{t}_n, \bar{x}_{m-1}) \right] \quad (m = 1, \dots, M-1), \\ c(\bar{t}_{n+1}, \bar{x}_0) &= c(\bar{t}_{n+1}, \bar{x}_1), & c(\bar{t}_{n+1}, \bar{x}_M) &= 1 \quad (n = 1, 2, \dots). \end{aligned} \quad (28)$$

To calculate the relative mass gain, the integral in Eq. (26) is approximated by the Euler formula

$$\Phi(\bar{t}_n) = \Delta x \sum_{m=0}^{M-1} c(\bar{t}_n, \bar{x}_m). \quad (29)$$

The coefficient  $\bar{D}$  is determined by the following procedure. We fix some interval  $[D_{\min}, D_{\max}]$ , where the “best-fit” value of  $\bar{D}$  is supposed to be located, and divide this interval into  $I$  sub-intervals by the points  $\bar{D}_i = D_{\min} + i\Delta D$  ( $i = 0, 1, \dots, I$ ), where  $\Delta D = (D_{\max} - D_{\min})/I$ . For any  $\bar{D}_i$ , Eq. (28) is solved numerically (with the steps  $\Delta x = 0.05$  and  $\Delta t = 0.005$  that ensure the stability of the numerical algorithm), and the function  $\Phi(\bar{t}_n)$  is given by Eq. (29). The “best-fit” value of  $\bar{D}$  is found from the condition of minimum of the function

$$F = \sum_{\bar{t}_k} \left[ \Phi_{\exp}(\bar{t}_k) - \Phi_{\text{num}}(\bar{t}_k) \right]^2,$$

where the sum is calculated over all point  $\bar{t}_k$  depicted in Figure 6,  $\Phi_{\exp}(\bar{t}_k)$  is the relative mass gain measured in the test, and  $\Phi_{\text{num}}(\bar{t}_k)$  is determined from Eq. (29). After the “best-fit” diffusivity,  $\bar{D}_i$ , is found, the procedure is repeated for the new interval  $[\bar{D}_{i-1}, \bar{D}_{i+1}]$  to guarantee an acceptable accuracy of matching observations. Figure 6 demonstrates fair agreement between the experimental data and the results of numerical simulation.

To ensure that the numerical results are independent of the choice of the steps of integration,  $\Delta x$  and  $\Delta t$ , we repeat integration of Eqs. (28) and (29) with the “best-fit” parameter  $\bar{D}$  and the new values  $\Delta x = 0.01$  and  $\Delta t = 0.0005$ . No difference was observed between the curve plotted in Figure 6 and the curve obtained by the numerical integration of Eqs. (28) and (29) with the decreased steps in time and the spatial coordinate.

The above procedure is repeated to match observations in the tests on 4 different samples. The average value of diffusivity is presented in Figure 13, where the vertical bars stand for the standard deviation.

It is worth noting that the algorithm of fitting experimental data used in this work differs from the conventional procedure employed by Shah et al. (2002), according to which the coefficient of diffusion was determined by matching the initial parts of the mass gain diagrams (where the function  $\Phi(\bar{t})$  is approximately linear).

The same numerical algorithm is employed to match experimental data on polymeric nanocomposites with various amounts of filler. The difference in the treatment of observations consists in the following: (i) Eq. (28) are replaced by the finite-difference approximation of Eqs. (17) and (19); (ii) the “best-fit” values are simultaneously determined for 3 adjustable parameters:  $\bar{D}$ ,  $C$  and  $K$ . Figures 7 to 10 show good agreement between the experimental data and the results of numerical analysis. The average values of  $D$  [this quantity is found from Eq. (18)],  $C$  and  $K$  (over 4 tests) are plotted versus the filler fraction,  $\nu$ , in Figures 13 to 15. The dependences of these parameters on the concentration of filler are approximated by the linear equations

$$D = D_0 - D_1\nu, \quad C = C_1\nu, \quad K = K_0 - K_1\nu, \quad (30)$$

where the coefficients  $D_j$ ,  $C_j$  and  $K_j$  ( $j = 0, 1$ ) are found by the least-squares technique.

It follows from Eq. (25) that the maximal moisture uptake per unit mass of the matrix,  $R_{\text{pol}} = \kappa n^0 / \rho$ , is given by

$$R_{\text{pol}} = \frac{R(\infty)}{1 + C}. \quad (31)$$

Using experimental data for  $R(\infty)$  and the values of  $C$  determined by matching observations, we calculate  $R_{\text{pol}}$  from Eq. (31) and plot this parameter versus the clay content in Figure 16.

## 7 Discussion

Figure 11 demonstrates that the elastic modulus,  $E$ , decreases with the clay content,  $\nu$ , in the region of small concentrations of filler ( $\nu < 1.0$  wt.-%), and remains practically constant when  $\nu$  exceeds 1.0 wt.-%. According to Figure 16, the filler fraction,  $\nu$ , affects the maximal moisture uptake,  $R_{\text{pol}}$ , in a similar way. These dependences of the parameters  $E$  and  $R_{\text{pol}}$  seem quite natural, because these quantities characterize the macro-response of a nanocomposite in tensile and diffusion tests. They may be explained by a progressive decrease in the degree of cross-linking with the growth of clay concentration (Bharadwaj et al., 2002), which results in a decrease in the number of active chains (whose ends are linked to nearby junctions) compared to the neat vinyl ester resin. This implies that the elastic modulus (proportional to the number of active chains) is reduced and the maximal weight gain (proportional to the free volume per unit active chains) is increased. Figures 11 and 16 show that the concentration of chains reaches its limiting value rather rapidly (when the filler content is about  $\nu_c = 1$  wt.-%), and an increase in the clay concentration above this critical value does not affect the cross-linking process.

Figure 12 demonstrates that the rate of developed plastic flow,  $a$ , strongly decreases with  $\nu$  in the region below the critical concentration of filler,  $\nu \leq \nu_c$ , and it weakly decreases with  $\nu$  when the clay content exceeds its critical value. Figures 13 and 15 reveal that the coefficient of diffusion,  $D$ , and the rate of adsorption of water molecules on surfaces of nano-layers,  $K$ , demonstrate similar dependences on the filler fraction. This behavior of the quantities  $a$ ,  $D$  and  $K$  appears to be in agreement with our physical intuition, because all these parameters reflect mobility of polymeric chains. According to Figures 12, 13 and 15, this mobility is drastically reduced with  $\nu$  in the sub-critical region, and it proceeds to decrease (however, rather weakly) when the filler content exceeds the critical concentration  $\nu_c$ . The conclusion that the mobility of chains in the polymeric matrix decreases with the clay content is also confirmed by DSC measurements (Shah et al., 2002) which reveal the the glass transition temperature monotonically increases with  $\nu$ .

Figure 14 reveals that the parameter  $C$  linearly increases with  $\nu$ . It follows from Figure 16 and Eqs. (25) and (31) that the maximal moisture content in the polymeric matrix,  $n^\circ$ , is independent of the clay fraction. This result together with Eq. (20) and Figure 14 implies that number of sites on the clay layers where water molecules are immobilized,  $n_1^\circ$ , linearly grows with the filler concentration. The latter assertion is in agreement with the main assumptions of our model (the total number of sites where the penetrant molecules are immobilized equals the product of the average number of these sites per particle by the number of clay particles), and it may be treated as a confirmation of the kinetic equations for the anomalous moisture diffusion.

The similarity in this behavior of the quantities  $a$ ,  $D$  and  $K$  as functions of the clay concentration,  $\nu$ , provides a way to substantially reduce the number of (time-consuming) moisture diffusion experiments. If the parameters  $a$  and  $D$  decrease with  $\nu$  in the same fashion (our analysis of observations on vinyl ester resin nanocomposite with MMT particles treated with vinyl benzine trimethyl ammonium chloride confirms this hypothesis), the function  $a(\nu)$  can be determined with a high level of accuracy in standard tensile tests, whereas only a few moisture diffusion tests are necessary to find the dependence of diffusivity on the clay content,  $D = D(\nu)$ .

## 8 Concluding remarks

Mechanical and diffusion tests have been performed on a nanocomposite with vinyl ester resin matrix and montmorillonite clay filler at room temperature. Experimental data in tensile tests demonstrate that the mechanical behavior of the neat vinyl ester resin is strongly elastoplastic, whereas an increase in the clay content results in a decrease in the plastic strain (due to the constrains on mobility of junctions between polymeric chains imposed by nano-particles). Observations in diffusion tests show that moisture diffusion in the neat resin is Fickian, whereas it becomes noticeably anomalous (non-Fickian) with the growth of the clay content. This transition is ascribed by adsorbtion (immobilization) of the penetrant molecules on surfaces of hydrophilic clay layers.

Constitutive models have been proposed to describe the elastoplastic response and anomalous moisture diffusion in a nanocomposite. Both models are determined by 3

adjustable parameters that are found by fitting the experimental data. Fair agreement is demonstrated between the observations and the results of numerical simulation.

The following conclusions are drawn:

1. A critical concentration of clay is found,  $\nu_c \approx 1$  wt.-%, corresponding to both mechanical and diffusion tests. The filler content,  $\nu$ , strongly affects the material constants in the sub-critical region, and its influence becomes rather weak in the post-critical domain.
2. The quantities independent of molecular mobility, such as the elastic modulus,  $E$ , and the maximal moisture uptake by the polymeric matrix,  $R_{pol}$ , are not affected by the concentration of clay particles when the filler content exceeds its critical value.
3. The quantities reflecting mobility of polymeric chains, such as the rate of developed plastic flow,  $a$ , the coefficient of diffusion,  $D$ , and the rate of moisture adsorption on nano-particles,  $k$ , strongly decrease with the filler content in the sub-critical region, and proceed to decrease (with smaller rates) at  $\nu > \nu_c$ .

## References

Bavisi BH, Pritchard G, Ghotra JS (1996) Measuring and reducing moisture penetration through thick laminates. *Adv. Polym. Technol.* 15: 223–235

Bharadwaj RK, Mehrabi AR, Hamilton C, Trujillo C, Murga M, Fan R, Chavira A, Thompson AK (2002) Structure–property relationships in cross-linked polyester–clay nanocomposites. *Polymer* 43: 3699–3705

Boyce MC, Parks DM, Argon AS (1988) Large inelastic deformation of glassy polymers. 1. Rate dependent constitutive model. *Mech. Mater.* 7: 15–33

Carter HG, Kibler KG (1978) Langmuir-type model for anomalous diffusion in composite resin. *J. Compos. Mater.* 12: 118–130

Cai LW, Weitsman Y (1994) Non-Fickian moisture diffusion in polymeric composites. *J. Compos. Mater.* 28: 130–154

Chang Y-W, Yang Y, Ryu S, Nah C (2002) Preparation and properties of EPDM/organo-montmorillonite hybrid nanocomposites. *Polym. Int.* 51: 310–324

Chen C, Han B, Li J, Shang T, Zou J, Jiang W (2001) A new model on the diffusion of small molecule penetrants in dense polymer membranes. *J. Membrane Sci.* 187: 109–118

Coulon G, Lefebvre JM, Escaig B (1986) The preyield evolution with strain of the work-hardening rate of glassy polymers (PABM resin). *J. Mater. Sci.* 21: 2059–2066

David L, Quinson R, Gauthier C, Perez J (1997) The role of anelasticity in high stress mechanical response and physical properties of glassy polymers. *Polym. Eng. Sci.* 37: 1633–1640

Drozdov AD (2001) The viscoelastic and viscoplastic responses of glassy polymers. *Int. J. Solids Structures* 38: 8259–8278

Gurtin ME, Yatomi C (1979) On a model for two phase diffusion in composite mateirals. *J. Compos. Mater.* 13: 126–130

Hasan OA, Boyce MC (1995) A constitutive model for the nonlinear viscoelastic viscoplastic behavior of glassy polymers. *Polym. Eng. Sci.* 35: 331–344

Kim TH, Jang LW, Lee DC, Choi HJ, Jhon MS (2002) Synthesis and rheology of intercalated polystyrene/Na<sup>+</sup>-montmorillonite nanocomposites. *Macromol. Rapid Commun.* 23: 191–195

Ma J, Qi Z, Hu Y (2001) Synthesis and characterization of polypropylene/clay nanocomposites. *J. Appl. Polym. Sci.* 82: 3611–3617

Mangion MBM, Cavaille JY, Perez J (1992) A molecular theory for the sub- $T_g$  plastic mechanical response of amorphous polymers. *Phil. Magazine A* 66: 773–796

Marcovich NE, Reboedo MM, Aranguren MI (1999) Moisture diffusion in polyester–woodflour composites. *Polymer* 40: 7313–7320

Masenelli-Varlot K, Reynard E, Vigier G, Varlet J (2002) Mechanical properties of clay-reinforced polyamide. *J. Polym. Sci. Part B: Polym. Phys.* 40: 272–283

Metzler R, Klafter J (2000) The random walk's guide to anomalous diffusion: a fractional

dynamics approach. *Phys. Rep.* 339: 1–77

Patel SV, Raval DK, Thakkar JR (1999) Novel vinyl ester resin and its urethane derivatives for glass reinforced composites. *Angew. Makromol. Chem.* 265: 13–15

Roy S, Xu, WX, Park SJ, Liechti KM (2000) Anomalous moisture diffusion in viscoelastic polymers: modeling and testing. *Trans. ASME. J. Appl. Mech.* 67: 391–396

Roy S, Xu W, Patel S, Case S (2001) Modeling of moisture diffusion in the presence of bi-axial damage in polymer matrix composite laminates. *Int. J. Solids Structures* 38: 7627–7641

Shah AP, Gupta RK, GangaRao HVS, Powell CE (2002) Moisture diffusion through vinyl ester nanocomposites made with montmorillonite clay. *Polym. Eng. Sci.* (accepted)

Tyan H-L, Wei K-H, Hsieh T-E (2000) Mechanical properties of clay-polyimide (BTDA-ODA) nanocomposites via ODA-modified organic clay. *J. Polym. Sci. Part B: Polym. Phys.* 38: 2873–2878

Valea A, Martinez I, Gonzalez ML, Eceiza A, Mondragon I (1998) Influence of cure schedule and solvent exposure on the dynamic mechanical behavior of a vinyl ester resin containing glass fibers. *J. Appl. Polym. Sci.* 70: 2595–2602

Vanlandingham MR, Eduljee RF, Gillespie JW (1999) Moisture diffusion in epoxy systems. *J. Appl. Polym. Sci.* 71: 787–798

Uschitsky M, Suhir E (2001) Moisture diffusion in epoxy molding compounds filled with particles. *Trans. ASME. J. Electronic Packaging* 123: 47–51

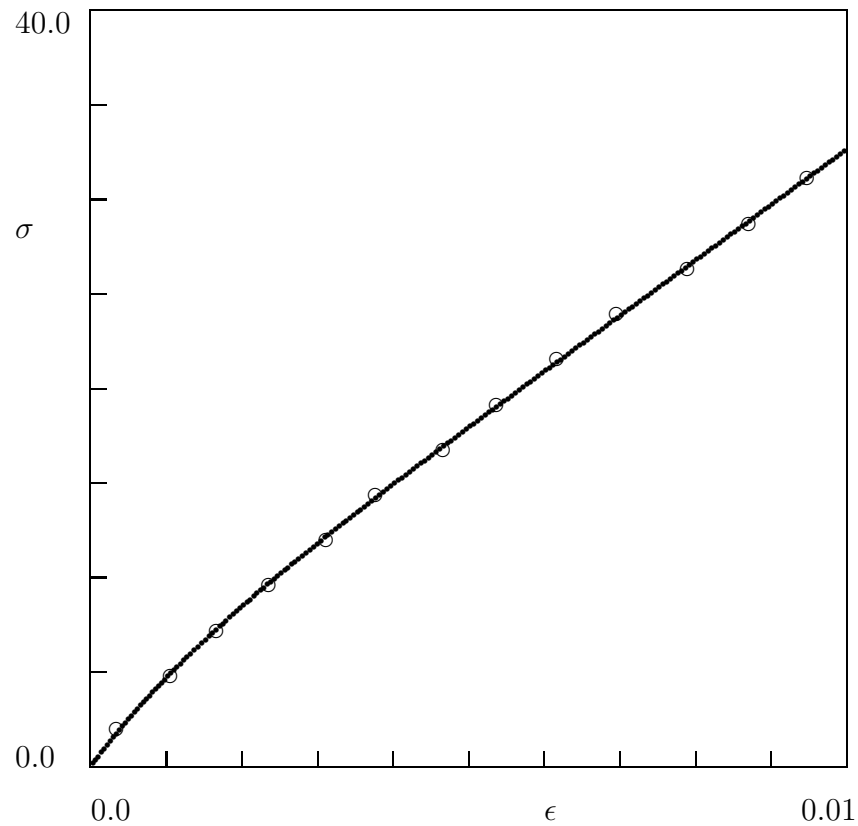


Figure 1: The stress  $\sigma$  MPa versus strain  $\epsilon$  for neat vinyl ester resin. Circles: experimental data. Solid line: results of numerical simulation

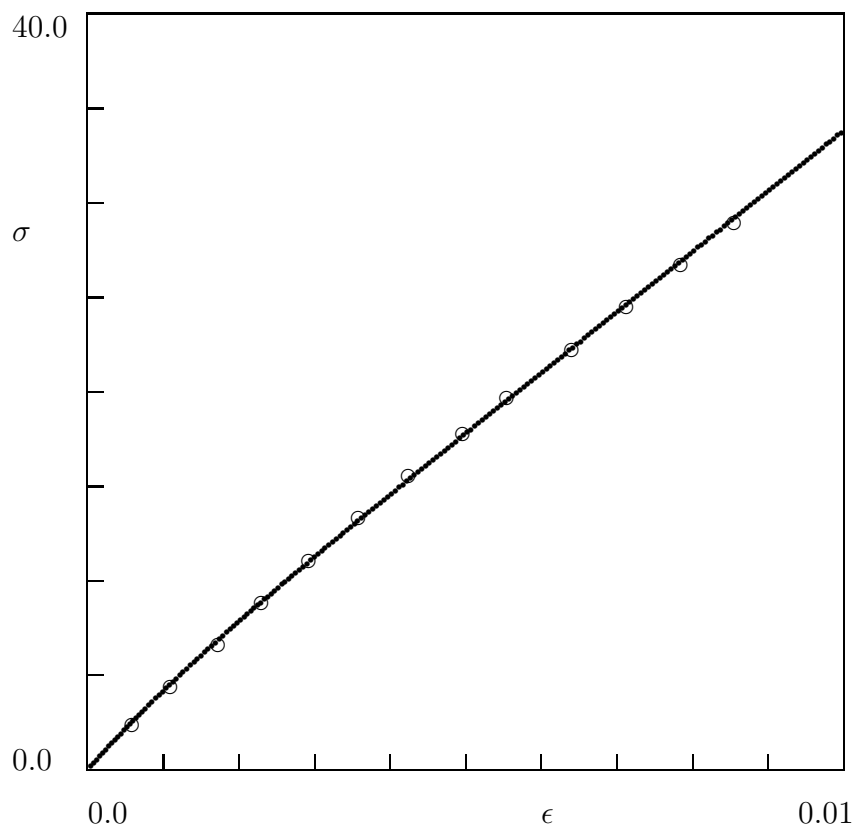


Figure 2: The stress  $\sigma$  MPa versus strain  $\epsilon$  for nanocomposite with  $\nu = 0.5$  wt.-%. Circles: experimental data. Solid line: results of numerical simulation

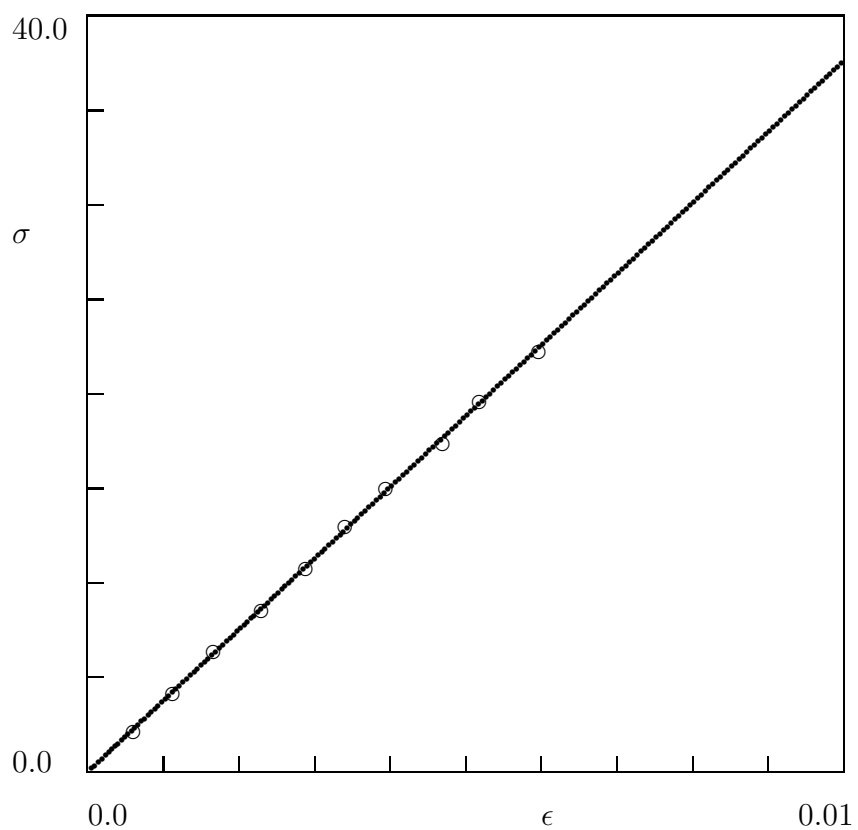


Figure 3: The stress  $\sigma$  MPa versus strain  $\epsilon$  for nanocomposite with  $\nu = 1.0$  wt.-%. Circles: experimental data. Solid line: results of numerical simulation

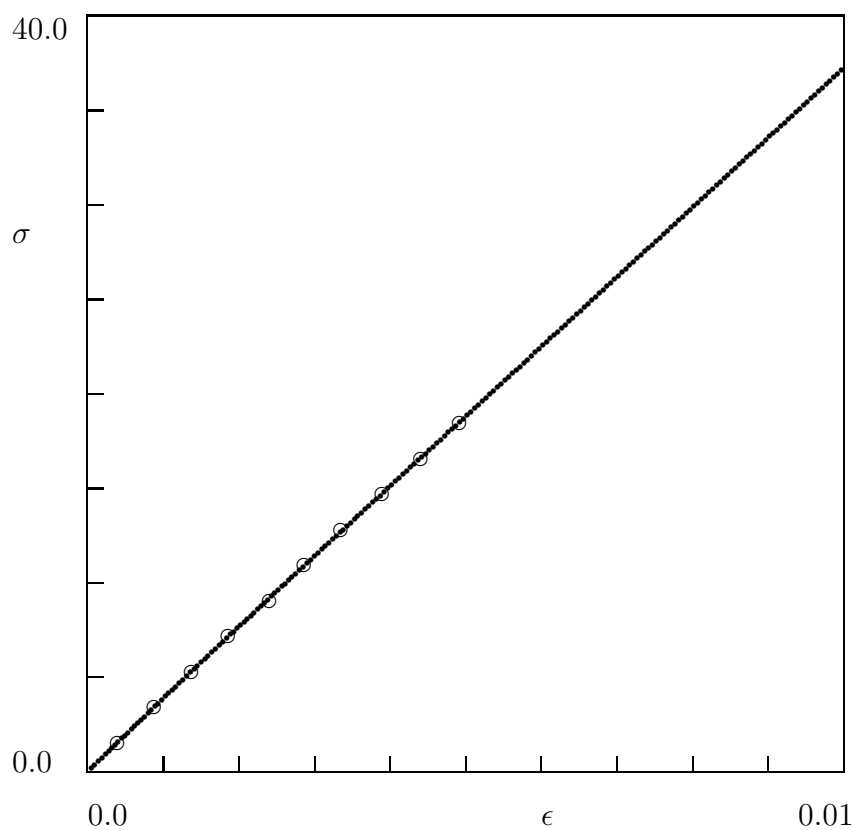


Figure 4: The stress  $\sigma$  MPa versus strain  $\epsilon$  for nanocomposite with  $\nu = 2.5$  wt.-%. Circles: experimental data. Solid line: results of numerical simulation

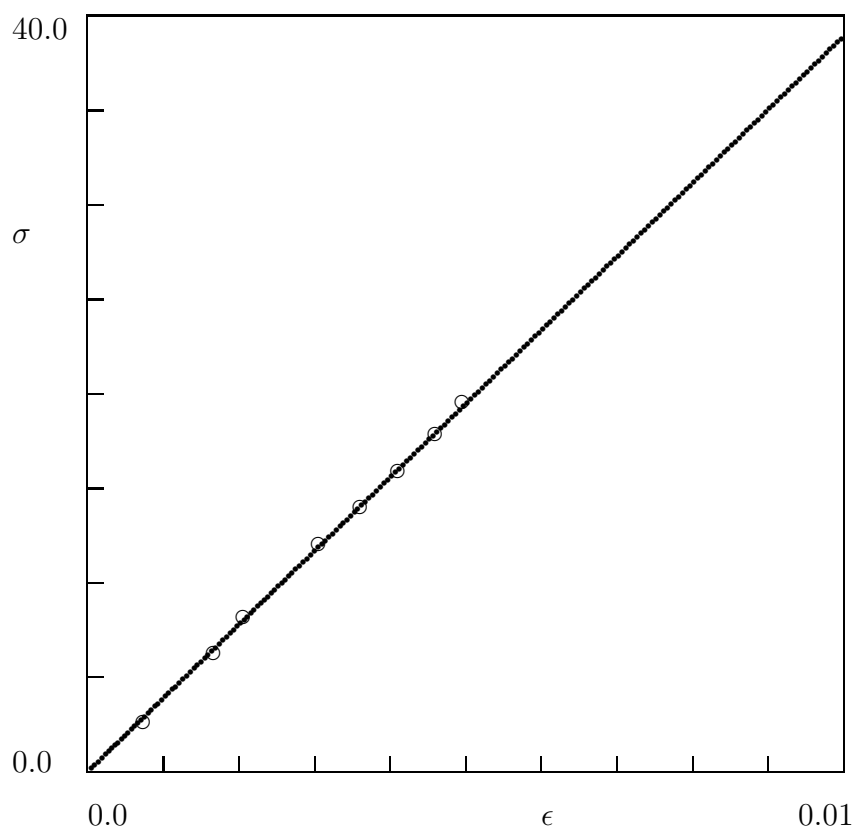


Figure 5: The stress  $\sigma$  MPa versus strain  $\epsilon$  for nanocomposite with  $\nu = 5.0$  wt.-%. Circles: experimental data. Solid line: results of numerical simulation

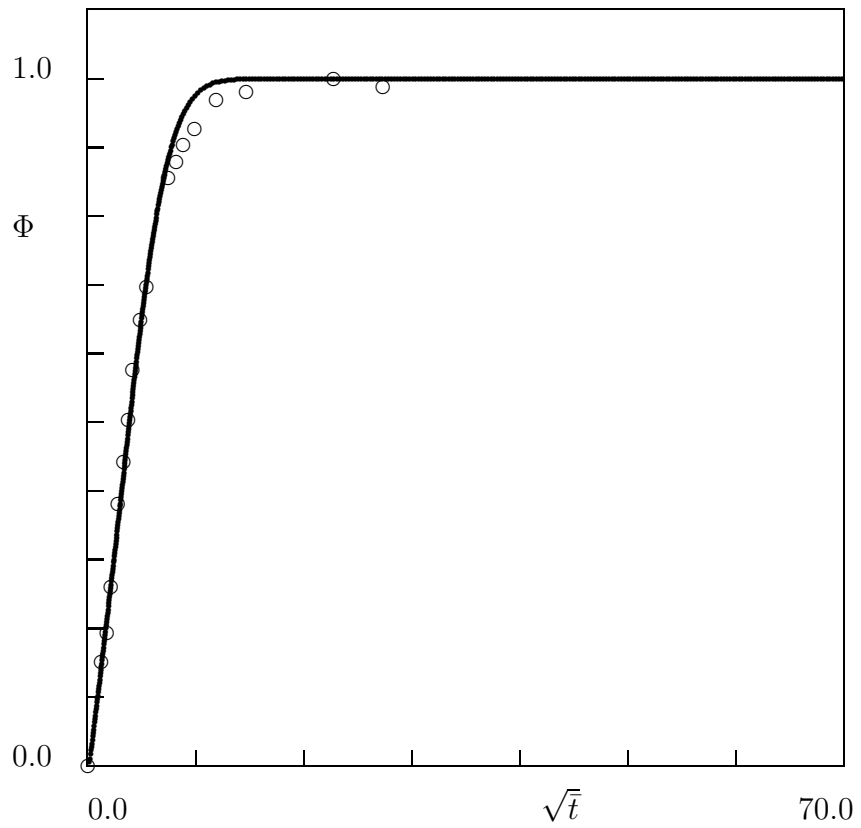


Figure 6: The relative moisture uptake  $\Phi$  versus the reduced time  $\bar{t}$  ( $\text{h}^{\frac{1}{2}}/\text{mm}$ ) for neat vinyl ester resin. Circles: experimental data ( $2l = 0.56726 \text{ mm}$ ). Solid line: results of numerical simulation

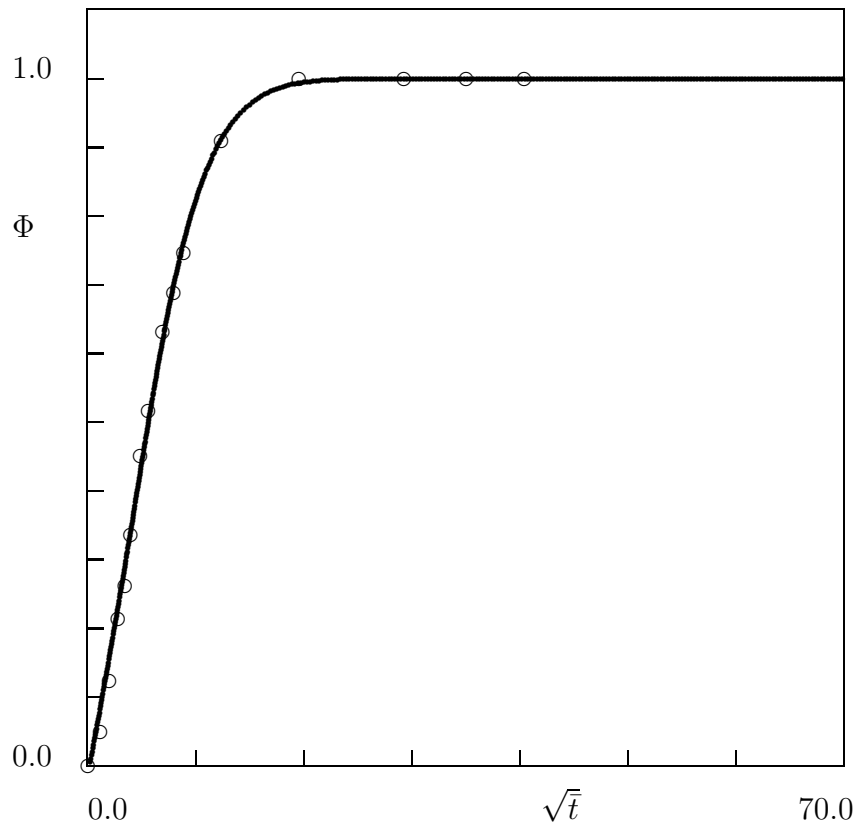


Figure 7: The relative moisture uptake  $\Phi$  versus the reduced time  $\bar{t}$  ( $\text{h}^{\frac{1}{2}}/\text{mm}$ ) for nanocomposite with  $\nu = 0.5$  wt.-%. Circles: experimental data ( $2l = 0.25373$  mm). Solid line: results of numerical simulation

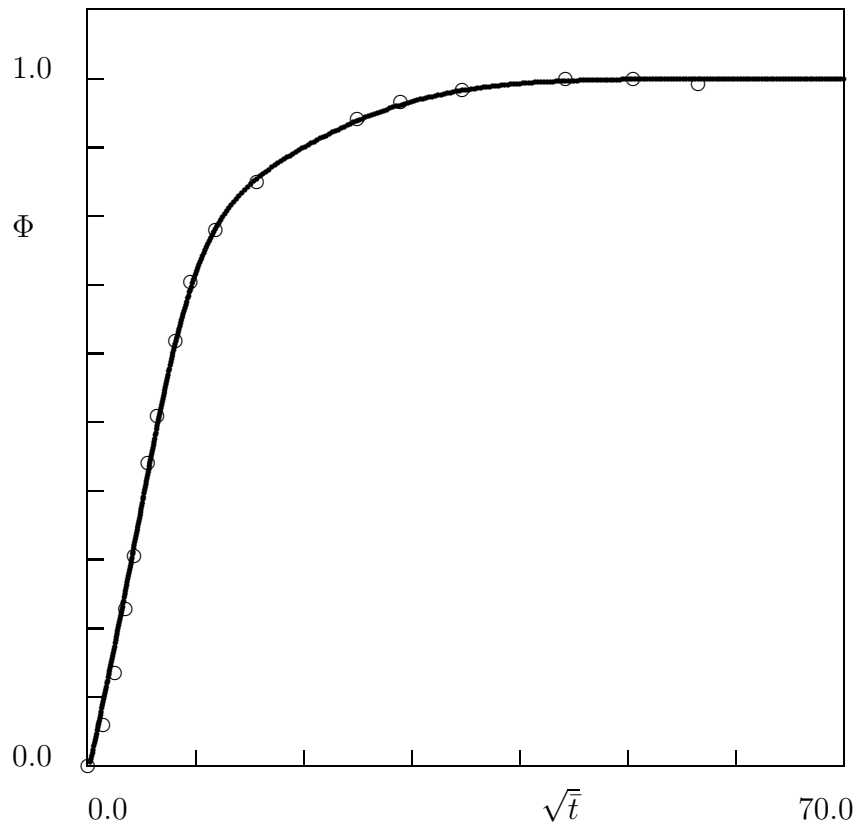


Figure 8: The relative moisture uptake  $\Phi$  versus the reduced time  $\bar{t}$  ( $\text{h}^{\frac{1}{2}}/\text{mm}$ ) for nanocomposite with  $\nu = 1.0$  wt.-%. Circles: experimental data ( $2l = 0.20108$  mm). Solid line: results of numerical simulation

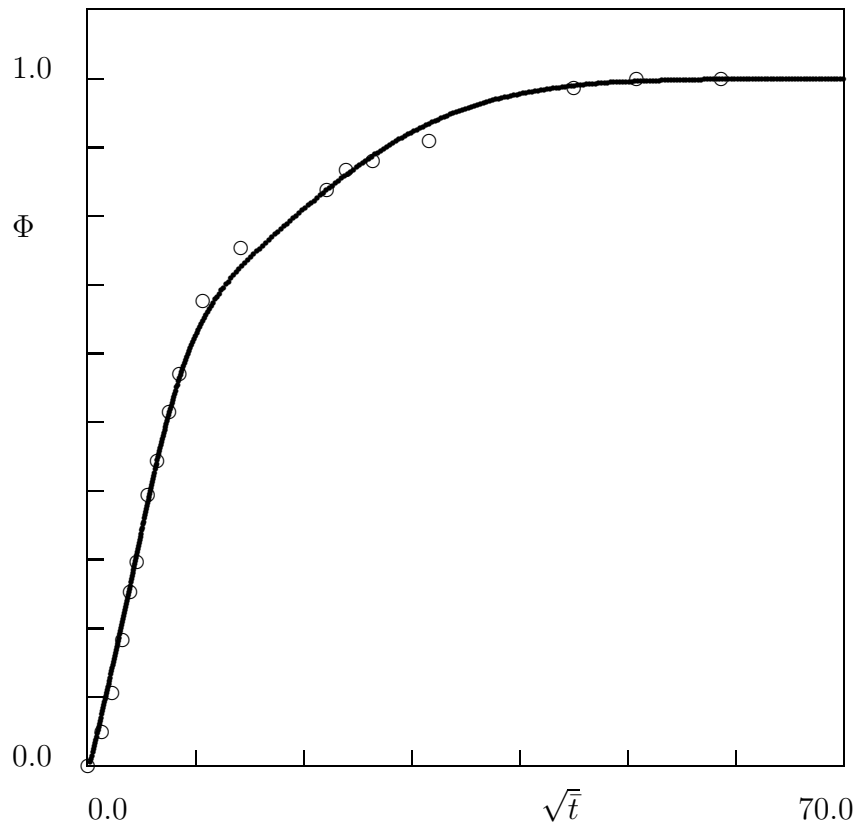


Figure 9: The relative moisture uptake  $\Phi$  versus the reduced time  $\bar{t}$  ( $\text{h}^{\frac{1}{2}}/\text{mm}$ ) for nanocomposite with  $\nu = 2.5$  wt.-%. Circles: experimental data ( $2l = 0.22013$  mm). Solid line: results of numerical simulation

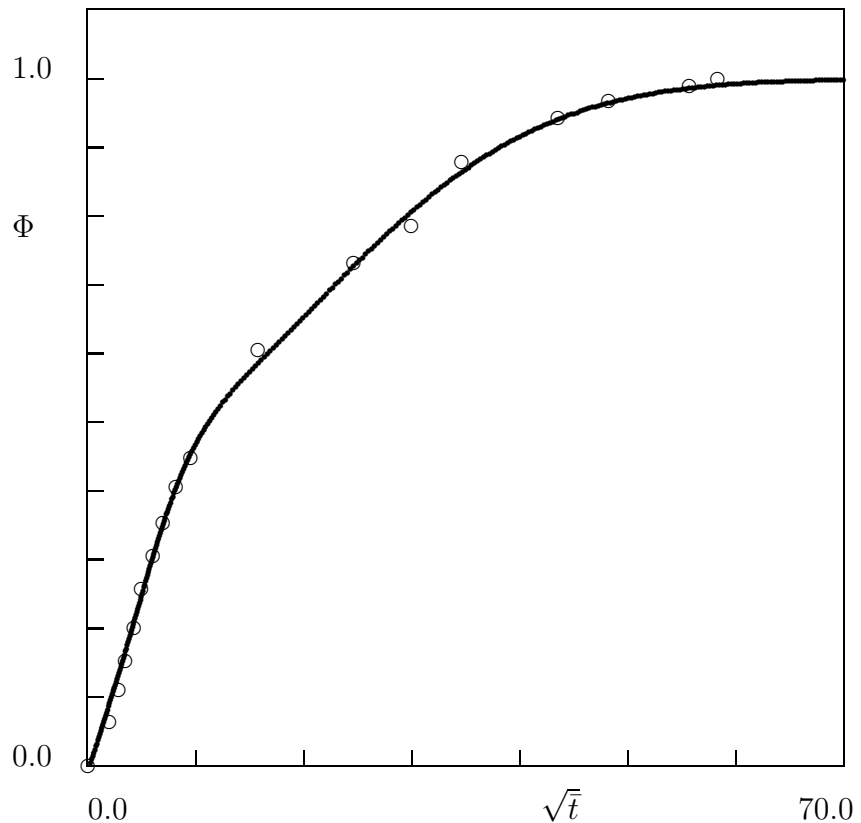


Figure 10: The relative moisture uptake  $\Phi$  versus the reduced time  $\bar{t}$  ( $\text{h}^{\frac{1}{2}}/\text{mm}$ ) for nanocomposite with  $\nu = 5.0$  wt.-%. Circles: experimental data ( $2l = 0.2032$  mm). Solid line: results of numerical simulation

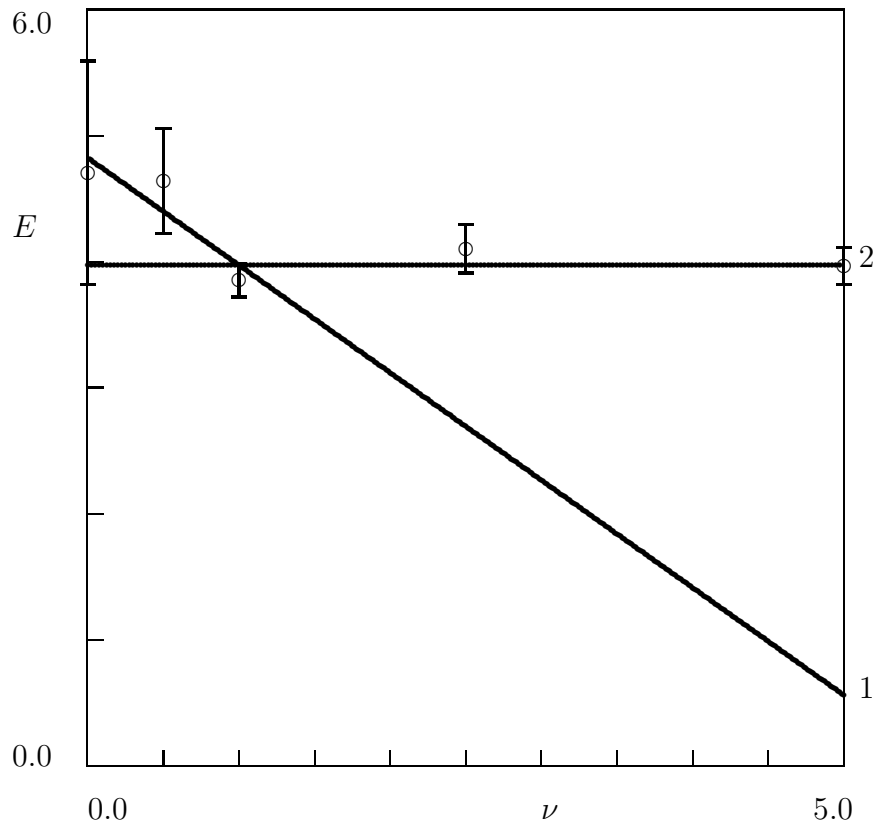


Figure 11: The elastic modulus  $E$  GPa versus the clay concentration  $\nu$  wt.-%. Circles: treatment of observations. Solid lines: approximation of the experimental data by Eq. (10). Curve 1:  $E_0 = 4.83$ ,  $E_1 = 0.85$ ; curve 2:  $E_0 = 3.97$ ,  $E_1 = 0.0$

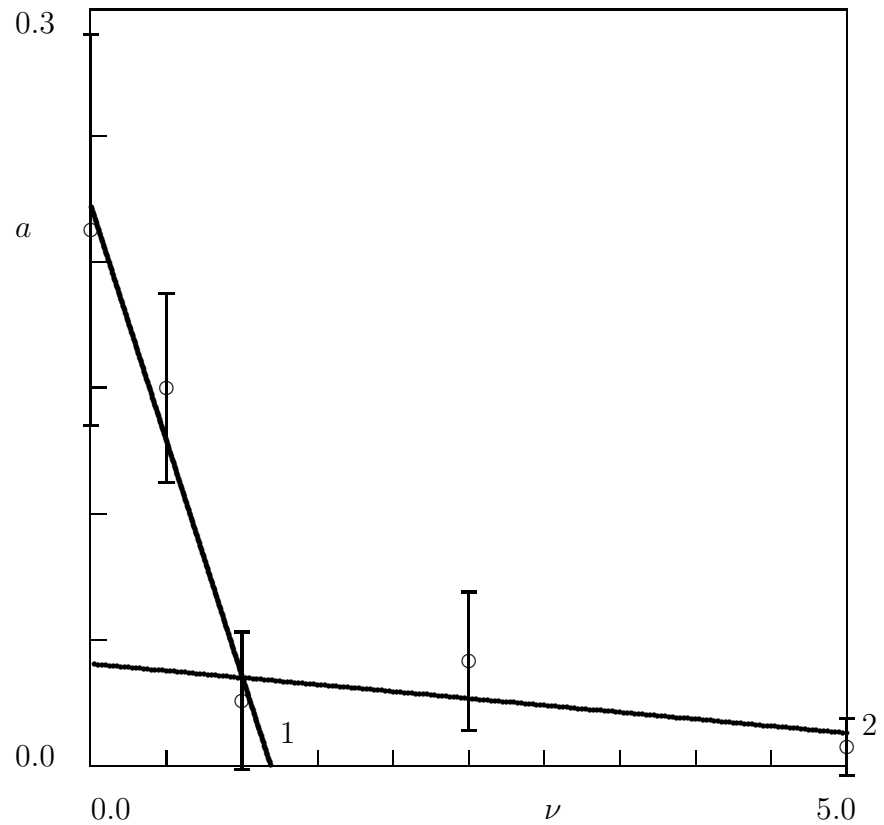


Figure 12: The rate of developed plastic flow  $a$  versus the clay concentration  $\nu$  wt.-%. Circles: treatment of observations. Solid lines: approximation of the experimental data by Eq. (10). Curve 1:  $a_0 = 0.22$ ,  $a_1 = 0.19$ ; curve 2:  $a_0 = 0.04$ ,  $a_1 = 0.01$

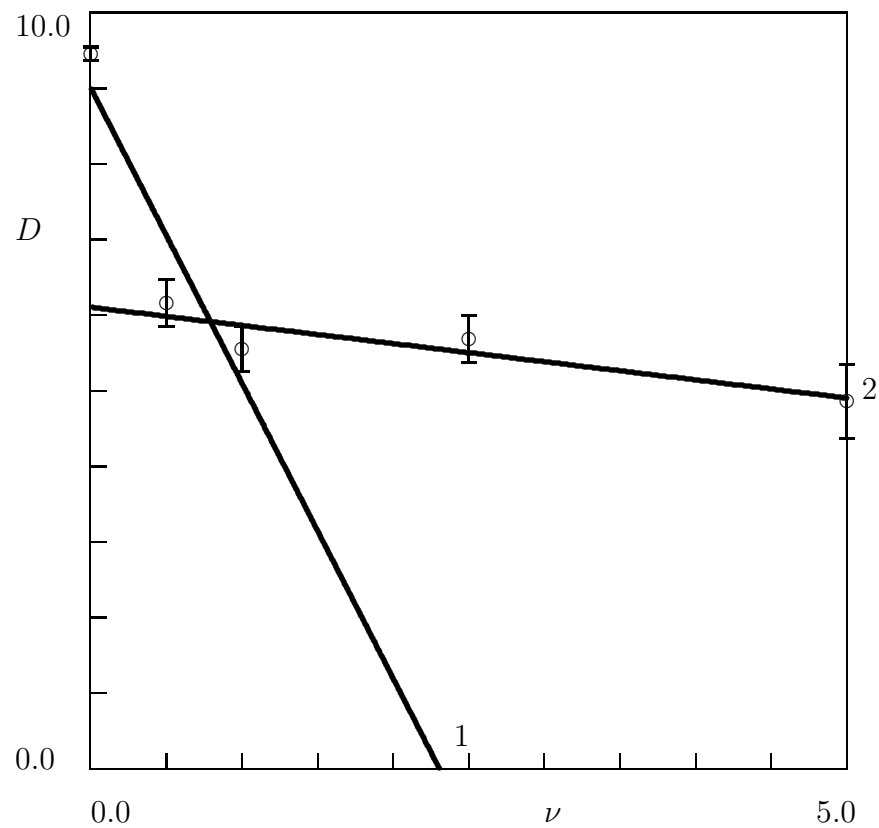


Figure 13: Diffusivity  $D \cdot 10^{-7}$  mm<sup>2</sup>/s versus the clay concentration  $\nu$  wt.-%. Circles: treatment of observations. Solid lines: approximation of the experimental data by Eq. (31). Curve 1:  $D_0 = 9.01$ ,  $D_1 = 3.91$ ; curve 2:  $D_0 = 6.11$ ,  $D_1 = 0.24$

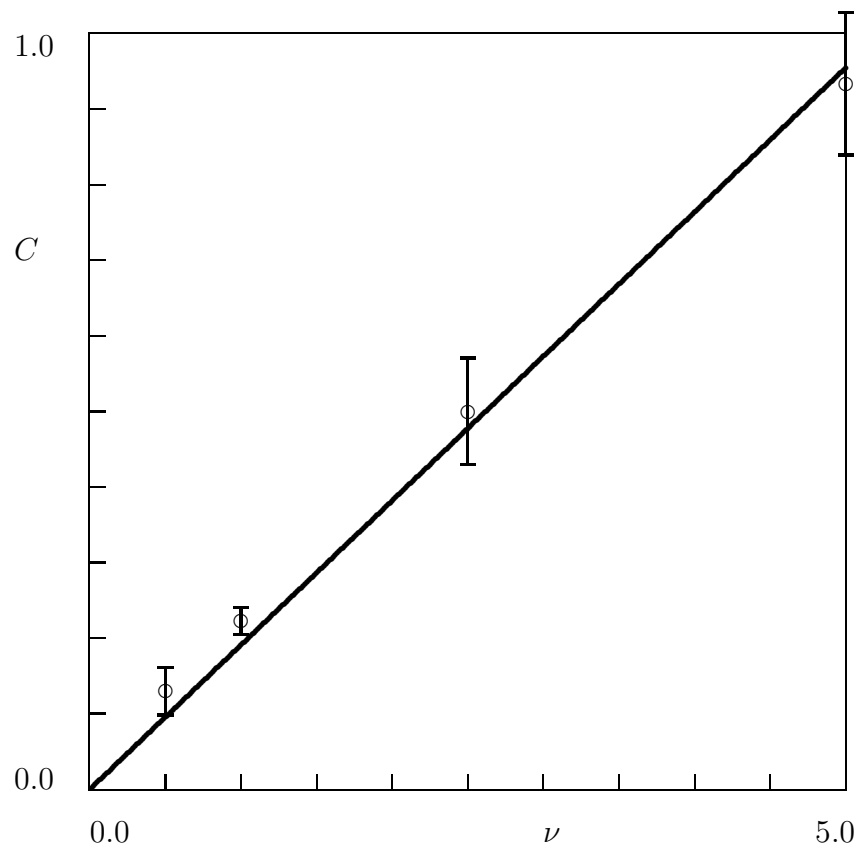


Figure 14: The dimensionless parameter  $C$  versus the clay concentration  $\nu$  wt.-%. Circles: treatment of observations. Solid line: approximation of the experimental data by Eq. (31) with  $C_1 = 0.19$

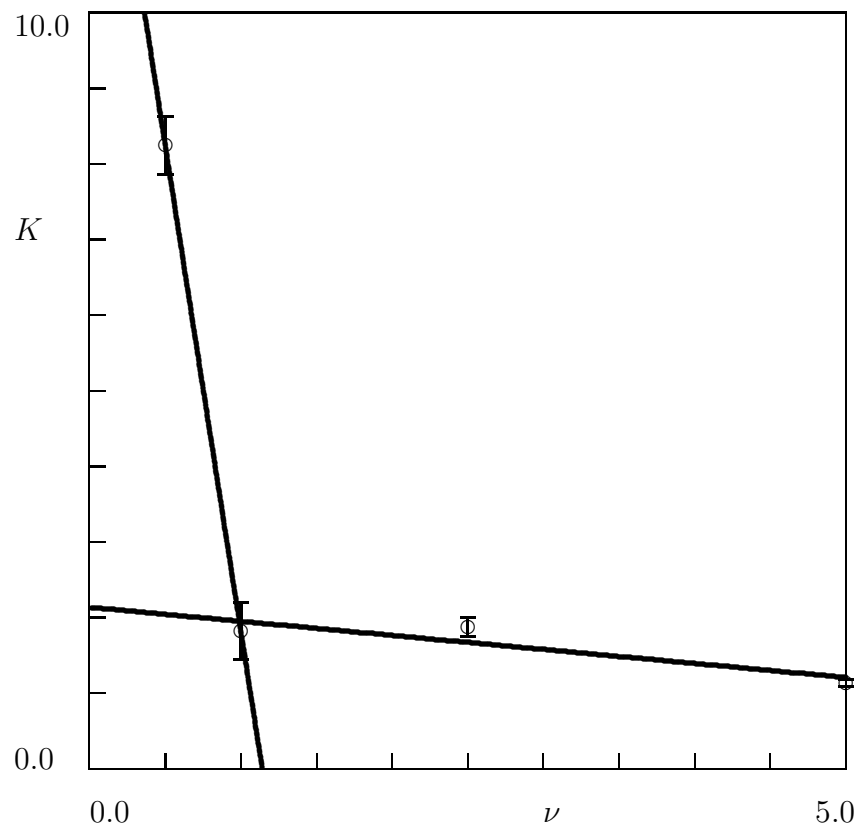


Figure 15: The adsorption rate  $K \cdot 10^{-3} \text{ h}^{-1}$  versus the clay concentration  $\nu$  wt.-%. Circles: treatment of observations. Solid lines: approximation of the experimental data by Eq. (31). Curve 1:  $K_0 = 14.68$ ,  $K_1 = 12.85$ ; curve 2:  $K_0 = 2.14$ ,  $K_1 = 0.19$

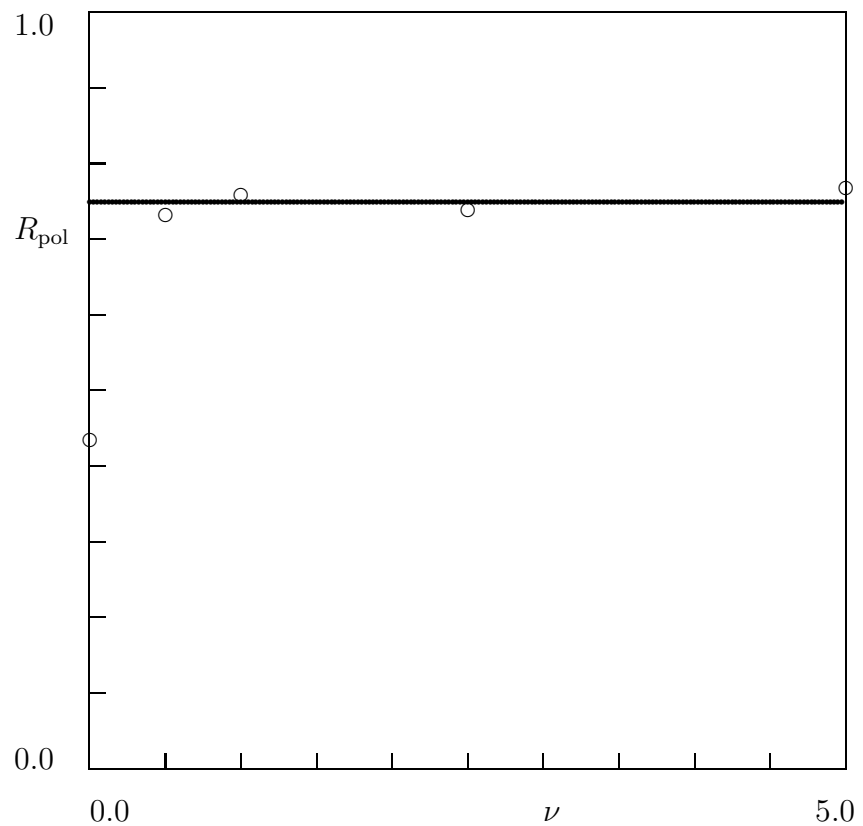


Figure 16: The maximal moisture uptake per unit mass of the matrix  $R_{\text{pol}}$  % versus the clay concentration  $\nu$  wt.-%. Circles: treatment of observations. Solid line: approximation of the experimental data by the constant  $R_{\text{pol}} = 0.75$  %